Due to a production error by the publisher, the second author was inadvertently credited with receiving an award in his biography in the paper (DOI: 10.1109/TIP.2010.2069690), entitled: "Distance Regularized Level Set Evolution and Its Application to Image Segmentation."

The biography should read:

Chenyang Xu (S'94–M'01–SM'06) received the B.S. degree in computer science and engineering from the University of Science and Technology of China, Hefei, in 1993 and the M.S.E. and Ph.D. degrees in electrical and computer engineering from the Johns Hopkins University, Baltimore, MD, in 1995 and 1999, respectively.

In 2000, he joined the Siemens Corporate Research, Princeton, NJ, as a member of technical staff. From 2006 to 2009, he was a Program Manager responsible for multimodality image fusion and image-guided solutions for interventional imaging applications. During the same time period, he cofounded and co-directed the Siemens Center for Medical Imaging Validation (CMIV), Beijing, China. Since July 2009, he has been the Chief Technology Officer at the Siemens Technology-To-Business (TTB) Center, Berkeley, CA. His research interests include image segmentation and registration, shape representation and analysis, deformable models, graph-based algorithms, statistical validation, and their applications in medical imaging, particularly intervention and minimal invasive surgery. He has authored or co-authored more than seventy research papers on these topics. According to Google Scholar, his top ten cited papers have received more than 4000 citations in total.

Dr. Xu is the co-inventor of the 3D imaging integration technology for Biosense-Webster's CARTOMERGE product, the world first commercial 3D imaging guidance product for treating complex heart arrhythmias. The technology was cited as a technological breakthrough in 2006 by Frost and Sullivan's Excellence in Technology Award to Biosense Webster Inc. Since 2005, tens of thousands of patients around the world have benefited from being treated using this technology.

Distance Regularized Level Set Evolution and Its Application to Image Segmentation

Chunming Li, Chenyang Xu, *Senior Member, IEEE*, Changfeng Gui, and Martin D. Fox, *Member, IEEE*

***Abstract*—Level set methods have been widely used in image processing and computer vision. In conventional level set formulations, the level set function typically develops irregularities during its evolution, which may cause numerical errors and eventually destroy the stability of the evolution. Therefore, a numerical remedy, called reinitialization, is typically applied to periodically replace the degraded level set function with a signed distance function. However, the practice of reinitialization not only raises serious problems as when and how it should be performed, but also affects numerical accuracy in an undesirable way. This paper proposes a new variational level set formulation in which the regularity of the level set function is intrinsically maintained during the level set evolution. The level set evolution is derived as the gradient flow that minimizes an energy functional with a distance regularization term and an external energy that drives the motion of the zero level set toward desired locations. The distance regularization term is defined with a potential function such that the derived level set evolution has a unique forward-and-backward (FAB) diffusion effect, which is able to maintain a desired shape of the level set function, particularly a signed distance profile near the zero level set. This yields a new type of level set evolution called distance regularized level set evolution (DRLSE). The distance regularization effect eliminates the need for reinitialization and thereby avoids its induced numerical errors. In contrast to complicated implementations of conventional level set formulations, a simpler and more efficient finite difference scheme can be used to implement the DRLSE formulation. DRLSE also allows the use of more general and efficient initialization of the level set function. In its numerical implementation, relatively large time steps can be used in the finite difference scheme to reduce the number of iterations, while ensuring sufficient numerical accuracy. To demonstrate the effectiveness of the DRLSE formulation, we apply it to an edge-based active contour model for image segmentation, and provide a simple narrowband implementation to greatly reduce computational cost.**

***Index Terms*—Forward and backward diffusion, image segmentation, level set method, narrowband, reinitialization.**

I. Introduction

THE LEVEL set method for capturing dynamic interfaces and shapes was introduced by Osher and Sethian [1] in 1987. The basic idea of the level set method is to represent a contour as the zero level set of a higher dimensional function, called a level set function (LSF), and formulate the motion of the contour as the evolution of the level set function. Some key ideas in the level set method were proposed earlier by Dervieux and Thomasset [2], [3] in the late 1970s, but their work did not draw much attention. It was only after the work by Osher and Sethian in [1], the level set method became well known and since then has had far-reaching impact in various applications, such as computational geometry, fluid dynamics, image processing, and computer vision.

In image processing and computer vision applications, the level set method was introduced independently by Caselles *et al.* [4] and Malladi *et al.* [5] in the context of active contour (or snake) models [6] for image segmentation. Early active contour models are formulated in terms of a dynamic parametric contour $\mathcal{C}(s,t) : [0,1]\times[0,\infty) \rightarrow \Re^2$ with a spatial parameter s in [0,1], which parameterizes the points in the contour, and a temporal variable $t \in [0,\infty)$. The curve evolution can be expressed as

$$\frac{\partial \mathcal{C}(s,t)}{\partial t} = F\mathcal{N} \tag{1}$$

where F is the speed function that controls the motion of the contour, and $\mathcal{N}$ is the inward normal vector to the curve $\mathcal{C}$. The curve evolution in (1) in terms of a parameterized contour can be converted to a level set formulation by embedding the dynamic contour $\mathcal{C}(s,t)$ as the zero level set of a time dependent LSF $\phi(x,y,t)$. Assuming that the embedding LSF ϕ takes negative values inside the zero level contour and positive values outside, the inward normal vector can be expressed as $\mathcal{N} = -\nabla\phi/|\nabla\phi|$, where ∇ is the gradient operator. Then, the curve evolution equation (1) is converted to the following partial differential equation (PDE):

$$\frac{\partial \phi}{\partial t} = F|\nabla\phi| \tag{2}$$

which is referred to as a level set evolution equation. The active contour model given in a level set formulation is called an implicit active contour or geometric active contour model. For specific active contours in parametric and their corresponding level set formulations, the readers are referred to [7].

A desirable advantage of level set methods is that they can represent contours of complex topology and are able to handle topological changes, such as splitting and merging, in a natural and efficient way, which is not allowed in parametric active contour models [6], [8], [9] unless extra indirect procedures are introduced in the implementations. Another desirable feature of level set methods is that numerical computations can be performed on a fixed Cartesian grid without having to parameterize the points on a contour as in parametric active contour models.

Manuscript received September 06, 2007; revised October 12, 2009; accepted October 12, 2009. Date of publication August 26, 2010; date of current version November 17, 2010. The associate editor coordinating the review of this manuscript and approving it for publication was Prof. Scott T. Acton.

C. Li is with Institute of Imaging Science, Vanderbilt University, Nashville, TN 37232 USA (e-mail: lchunming@gmail.com).

C. Xu is with Technology to Business Center, Siemens Corporate Research, Berkeley, CA 94704 USA (e-mail: chenyang.xu@siemens.com).

C. Gui is with Department of Mathematics, University of Connecticut, Storrs, CT 06269 USA (e-mail: gui@math.uconn.edu).

M. D. Fox is with Department of Electrical and Computer Engineering, University of Connecticut, Storrs, CT 06269 USA (e-mail: fox@engr.uconn.edu).

Digital Object Identifier 10.1109/TIP.2010.2069690

These desirable features, among others, have greatly promoted further development of level set methods and their applications in image segmentation [10]–[12], [7], [13]–[16], tracking [14], [17], and stereo reconstruction [18], etc.

Although level set methods have been used to solve a wide range of scientific and engineering problems, their applications have been plagued with the irregularities of the LSF that are developed during the level set evolution. In conventional level set methods, the LSF typically develops irregularities during its evolution (see the lower row of Fig. 3 for an example), which cause numerical errors and eventually destroy the stability of the level set evolution. To overcome this difficulty, a numerical remedy, commonly known as reinitialization [19], [20], was introduced to restore the regularity of the LSF and maintain stable level set evolution. Reinitialization is performed by periodically stopping the evolution and reshaping the degraded LSF as a signed distance function [21], [20].

A standard method for reinitialization is to solve the following evolution equation to steady state:

$$\frac{\partial \psi}{\partial t} = \mathrm{sign}(\phi)(1 - |\nabla \psi|) \tag{3}$$

where ϕ is the LSF to be reinitialized, and $\mathrm{sign}(\cdot)$ is the sign function. Ideally, the steady state solution of this equation is a signed distance function. This reinitialization method has been widely used in level set methods [21], [22]. Another method for reinitialization is the fast marching algorithm [19]. Although reinitialization as a numerical remedy is able to maintain the regularity of the LSF, it may incorrectly move the zero level set away from the expected position [20], [23], [19]. Therefore, reinitialization should be avoided as much as possible [19, p. 140].

Moreover, there are serious theoretical and practical problems in conventional level set formulations regarding the practice of reinitialization. Level set evolution equations in conventional level set formulations can be written in the form of (2) with a speed function F. The speed function F, which is defined to guide the motion of the zero level set, does not have a component for preserving the LSF ϕ as a signed distance function. In theory, it has been proven by Barles *et al.* [24] that the solutions to such Hamilton-Jacobi equations is not a signed distance function. However, the LSF is forced to be a signed distance function as a result of reinitialization. This is obviously a disagreement between theory and its implementation, as pointed out by Gomes and Faugeras [25]. From a practical viewpoint, the use of reinitialization introduces some fundamental problems yet to be solved, such as when and how to apply the reinitialization [25]. There are no general answers to these problems so far [23] and, therefore, reinitialization is often applied in an ad hoc manner.

Due to the previously mentioned theoretical and practical problems associated with reinitialization, it is necessary to pursue a level set method that does not require reinitialization. Gomes and Faugeras [25] proposed a level set formulation that consists of three PDEs, one of which is introduced to restrict the LSF to be a signed distance function, and the other two of which describe the motion of the zero level contour. However, it is not clear whether there exists a solution to this system of three PDEs in theory. Moreover, the numerical implementation of this formulation still causes errors that may destroy the signed distance property and eventually destabilize the level set evolution, which renders it necessary to introduce separate reinitialization procedures, as reported in [26]. Weber *et al.* [26] proposed an implementation strategy to avoid separate reinitialization procedures in their implementation of the well-known geodesic active contour (GAC) model in [11]. The updating of the LSF at each time step is performed by a complex procedure of solving an optimization problem, instead of an iteration scheme derived from the underlying evolution equation, which is a disagreement between the theory and its implementation. In our preliminary work [27], we proposed a variational level set formulation with an intrinsic mechanism of maintaining the signed distance property of the LSF. This mechanism is associated with a penalty term in the variational formulation that penalizes the deviation of the LSF from a signed distance function. The penalty term not only eliminates the need for reinitialization, but also allows the use of a simpler and more efficient numerical scheme in the implementation than those used for conventional level set formulations. However, this penalty term may cause an undesirable side effect on the LSF in some circumstances, which may affect the numerical accuracy.

This paper proposes a more general variational level set formulation with a distance regularization term and an external energy term that drives the motion of the zero level contour toward desired locations. The distance regularization term is defined with a potential function such that it forces the gradient magnitude of the level set function to one of its minimum points, thereby maintaining a desired shape of the level set function, particularly a signed distance profile near its zero level set. In particular, we provide a double-well potential for the distance regularization term. The level set evolution is derived as a gradient flow that minimizes this energy functional. In the level set evolution, the regularity of the LSF is maintained by a forward-and-backward (FAB) diffusion derived from the distance regularization term. As a result, the distance regularization completely eliminates the need for reinitialization in a principled way, and avoids the undesirable side effect introduced by the penalty term in our preliminary work [27]. We call the level set evolution in our formulation a distance regularized level set evolution (DRLSE). To demonstrate the effectiveness of the DRLSE formulation, we apply it to an edge-based active contour model for image segmentation. We provide a simple and efficient narrowband implementation to further improve the computational efficiency. Due to the distance regularization term, the DRLSE can be implemented with a simpler and more efficient numerical scheme in both full domain and narrowband implementations than conventional level set formulations. Moreover, relatively large time steps can be used to significantly reduce the number of iterations and computation time, while ensuring sufficient numerical accuracy.

This paper is organized as follows. In Section II, we first propose a general variational level set formulation with a distance regularization term. In Section III, we apply the proposed general formulation to an edge-based model for image segmentation, and describe its implementations in full domain and narrowband. Experimental results are shown in Section IV. Our work is summarized in Section V.

II. DRLSE

In level set methods, a contour (or more generally a hypersurface) of interest is embedded as the zero level set of an LSF. Although the final result of a level set method is the zero level set of the LSF, it is necessary to maintain the LSF in a good condition, so that the level set evolution is stable and the numerical computation is accurate. This requires that the LSF is smooth and not too steep or too flat (at least in a vicinity of its zero level set) during the level set evolution. This condition is well satisfied by signed distance functions for their unique property $|\nabla\phi| = 1$, which is referred to as the signed distance property. For the 2-D case as an example, we consider a signed distance function $z = \phi(x, y)$ as a surface. Then, its tangent plane makes an equal angle of 45° with both the xy-plane and the z-axis, which can be easily verified by the signed distance property $|\nabla\phi| = 1$. For this desirable property, signed distance functions have been widely used as level set functions in level set methods. In conventional level set formulations, the LSF is typically initialized and periodically reinitialized as a signed distance function. In this section, we propose a level set formulation that has an intrinsic mechanism of maintaining this desirable property of the LSF.

A. Energy Formulation With Distance Regularization

Let $\phi : \Omega \to \Re$ be a LSF defined on a domain Ω. We define an energy functional $\mathcal{E}(\phi)$ by

$$\mathcal{E}(\phi) = \mu\mathcal{R}_p(\phi) + \mathcal{E}_{\text{ext}}(\phi) \tag{4}$$

where $\mathcal{R}_p(\phi)$ is the level set regularization term defined in the following, $\mu > 0$ is a constant, and $\mathcal{E}_{\text{ext}}(\phi)$ is the external energy that depends upon the data of interest (e.g., an image for image segmentation applications). The level set regularization term $\mathcal{R}_p(\phi)$ is defined by

$$\mathcal{R}_p(\phi) \triangleq \int_\Omega p(|\nabla\phi|)d\mathbf{x} \tag{5}$$

where p is a potential (or energy density) function $p : [0, \infty) \to \Re$. The energy $\mathcal{E}_{\text{ext}}(\phi)$ is designed such that it achieves a minimum when the zero level set of the LSF ϕ is located at desired position (e.g., an object boundary for image segmentation applications). An external energy will be defined in Section III in an application of the general formulation (4) to image segmentation. The minimization of the energy $\mathcal{E}(\phi)$ can be achieved by solving a level set evolution equation, which will be given in Section II-B.

A naive choice of the potential function is $p(s) = s^2$ for the regularization term $\mathcal{R}_p$, which forces $|\nabla\phi|$ to be zero. Such a level set regularization term has a strong smoothing effect, but it tends to flatten the LSF and finally make the zero level contour disappear. In fact, the purpose of imposing the level set regularization term is not only to smooth the LSF ϕ, but also to maintain the signed distance property $|\nabla\phi| = 1$, at least in a vicinity of the zero level set, in order to ensure accurate computation for curve evolution. This goal can be achieved by using a potential function $p(s)$ with a minimum point $s = 1$, such that the level set regularization term $\mathcal{R}_p(\phi)$ is minimized when $|\nabla\phi| = 1$. Therefore, the potential function $p(s)$ should have a minimum point at $s = 1$ (it may have other minimum points). We will use such a potential p in the proposed variational level set formulation (4). The corresponding level set regularization term $\mathcal{R}_p(\phi)$ is referred to as a distance regularization term for its role of maintaining the signed distance property of the LSF. A simple and straightforward definition of the potential p for distance regularization is

$$p = p_1(s) \triangleq \frac{1}{2}(s-1)^2 \tag{6}$$

which has $s = 1$ as the unique minimum point. With this potential $p = p_1(s)$, the level set regularization term $\mathcal{R}_p(\phi)$ can be explicitly expressed as

$$\mathcal{P}(\phi) = \frac{1}{2}\int_\Omega (|\nabla\phi| - 1)^2 d\mathbf{x} \tag{7}$$

which characterizes the deviation of ϕ from a signed distance function.

The energy functional $\mathcal{P}(\phi)$ was proposed as a penalty term in our preliminary work [27] in an attempt to maintain the signed distance property in the entire domain. However, the derived level set evolution for energy minimization has an undesirable side effect on the LSF ϕ in some circumstances, which will be described in Section II-D. To avoid this side effect, we introduce a new potential function p in the distance regularization term $\mathcal{R}_p$. This new potential function is aimed to maintain the signed distance property $|\nabla\phi| = 1$ only in a vicinity of the zero level set, while keeping the LSF as a constant, with $|\nabla\phi| = 0$, at locations far away from the zero level set. To maintain such a profile of the LSF, the potential function $p(s)$ must have minimum points at $s = 1$ and $s = 0$. Such a potential is a double-well potential as it has two minimum points (wells). A double-well potential $p = p_2$ will be explicitly defined in Section II-C. Using this double-well potential $p = p_2$ not only avoids the side effect that occurs in the case of $p = p_1$, but also offers some appealing theoretical and numerical properties of the level set evolution, as will be seen in the rest of this paper.

B. Gradient Flow for Energy Minimization

In calculus of variations [28], a standard method to minimize an energy functional $\mathcal{F}(\phi)$ is to find the steady state solution of the gradient flow equation

$$\frac{\partial\phi}{\partial t} = -\frac{\partial\mathcal{F}}{\partial\phi} \tag{8}$$

where $\partial\mathcal{F}/\partial\phi$ is the Gâteaux derivative of the functional $\mathcal{F}(\phi)$. This is an evolution equation of a time-dependent function $\phi(\mathbf{x}, t)$ with a spatial variable $\mathbf{x}$ in the domain Ω and a temporal variable $t \geq 0$, and the evolution starts with a given initial function $\phi(\mathbf{x}, 0) = \phi_0(\mathbf{x})$. The evolution of the time-dependent function $\phi(\mathbf{x}, t)$ is in the opposite direction of the Gâteaux derivative, i.e., $-\partial\mathcal{F}/\partial\phi$, which is the steepest descent direction of the functional $\mathcal{F}(\phi)$. Therefore, the gradient flow is also called steepest descent flow or gradient descent flow.

The Gâteaux derivative of the functional $\mathcal{R}_p(\phi)$ in (5) is

$$\frac{\partial\mathcal{R}_p}{\partial\phi} = -\text{div}(d_p(|\nabla\phi|)\nabla\phi) \tag{9}$$

where $\mathrm{div}(\cdot)$ is the divergence operator and d_p is a function defined by

$$d_p(s) \triangleq \frac{p'(s)}{s}. \tag{10}$$

From (4) and the linearity of Gâteaux derivative, we have

$$\frac{\partial \mathcal{E}}{\partial \phi} = \mu \frac{\partial \mathcal{R}_p}{\partial \phi} + \frac{\partial \mathcal{E}_{\mathrm{ext}}}{\partial \phi} \tag{11}$$

where $\partial \mathcal{E}_{\mathrm{ext}}/\partial \phi$ is the Gâteaux derivative of the external energy functional $\mathcal{E}_{\mathrm{ext}}$ with respect to ϕ. Then, the gradient flow of the energy $\mathcal{E}(\phi)$ is

$$\frac{\partial \phi}{\partial t} = -\mu \frac{\partial \mathcal{R}_p}{\partial \phi} - \frac{\partial \mathcal{E}_{\mathrm{ext}}}{\partial \phi} \tag{12}$$

which, combined with (9), can be further expressed as

$$\frac{\partial \phi}{\partial t} = \mu \mathrm{div}\left(d_p(|\nabla \phi|)\nabla \phi\right) - \frac{\partial \mathcal{E}_{\mathrm{ext}}}{\partial \phi}. \tag{13}$$

This PDE is the level set evolution equation derived from the proposed variational formulation (4). We solve this PDE with the Neumann boundary condition [29] and a given initial function ϕ_0. We call the level set evolution (13) a DRLSE for its intrinsic capability of preserving the signed distance property of the LSF, which is associated with the distance regularization term $\mathcal{R}_p$ in (4). Reinitialization is not needed in the implementation of DRLSE due to the intrinsic distance regularization effect embedded in the level set evolution, as described in the following. The level set evolution without reinitialization in our preliminary work [27] is a special case of the DRLSE in (13).

The distance regularization effect in DRLSE can be seen from the gradient flow of the energy $\mu \mathcal{R}_p(\phi)$

$$\frac{\partial \phi}{\partial t} = \mu \mathrm{div}(d_p(|\nabla \phi|)\nabla \phi). \tag{14}$$

This flow can be expressed in standard form of a diffusion equation

$$\frac{\partial \phi}{\partial t} = \mathrm{div}(D \nabla \phi)$$

with diffusion rate $D = \mu d_p(|\nabla \phi|)$. Therefore, the flows in (13) and (14) have a diffusion effect on the level set function ϕ. This diffusion is not a usual diffusion, as the diffusion rate $\mu d_p(|\nabla \phi|)$ can be positive or negative for the potential p used in DRLSE. When $d_p(|\nabla \phi|)$ is positive, the diffusion is forward diffusion, which decreases $|\nabla \phi|$. When $d_p(|\nabla \phi|)$ is negative, the diffusion is backward diffusion, which increases $|\nabla \phi|$. Such diffusion is called a forward-and-backward (FAB) diffusion. This FAB diffusion adaptively increases or decreases $|\nabla \phi|$ to force it to be close to one of the minimum points of the potential function $p(s)$, thereby maintaining the desired shape of the function ϕ.

For the potential $p = p_1(s)$ defined in (6), we have $d_p(s) = 1 - (1/s)$. In this case, the PDE in (13) can be expressed as

$$\frac{\partial \phi}{\partial t} = \mu \left[\nabla^2 \phi - \mathrm{div}\left(\frac{\nabla \phi}{|\nabla \phi|}\right)\right] - \frac{\partial \mathcal{E}_{\mathrm{ext}}}{\partial \phi} \tag{15}$$

where ∇^2 is the Laplace operator. Note that the term $\mathrm{div}(\nabla \phi/|\nabla \phi|)$ computes the mean curvature of the level contours of the function ϕ.

The sign of the function $d_p(s) = 1 - (1/s)$ indicates the property of the FAB diffusion term in the following two cases:

- for $|\nabla \phi| > 1$, the diffusion rate $\mu d_p(|\nabla \phi|)$ is positive, and the diffusion (14) is forward, which decreases $|\nabla \phi|$;
- for $|\nabla \phi| < 1$, the diffusion rate $\mu d_p(|\nabla \phi|)$ is negative, and the diffusion becomes backward, which increases $|\nabla \phi|$.

Therefore, the FAB diffusion with potential $p = p_1$ forces $|\nabla \phi|$ to 1 to maintain the signed distance property. However, this FAB diffusion has an unbounded diffusion rate $\mu d_p(|\nabla \phi|) = \mu(1 - (1/|\nabla \phi|))$, which goes to negative infinity as $|\nabla \phi|$ approaches 0. This may cause an undesirable side effect on the LSF ϕ when $|\nabla \phi|$ is close to 0, as will be described in Section II-D. This side effect can be avoided by using a double-well potential $p = p_2$ defined next, for which the diffusion rate $\mu d_p(|\nabla \phi|)$ is bounded by a constant.

C. Double-Well Potential for Distance Regularization

As mentioned in Section II-A, a preferable potential function p for the distance regularization term $\mathcal{R}_p$ is a double-well potential. Here, we provide a specific construction of the double-well potential $p_2(s)$ as

$$p_2(s) = \begin{cases} \frac{1}{(2\pi)^2}(1 - \cos(2\pi s)), & \text{if } s \le 1 \\ \frac{1}{2}(s-1)^2, & \text{if } s \ge 1. \end{cases} \tag{16}$$

This potential $p_2(s)$ has two minimum points at $s = 0$ and $s = 1$.

It is easy to verify that p_2 is twice differentiable in $[0, \infty)$, with the first and second derivatives given by

$$p_2'(s) = \begin{cases} \frac{1}{2\pi}\sin(2\pi s), & \text{if } s \le 1 \\ s - 1, & \text{if } s \ge 1 \end{cases}$$

and

$$p_2''(s) = \begin{cases} \cos(2\pi s), & \text{if } s \le 1 \\ 1, & \text{if } s \ge 1. \end{cases}$$

The function $p_2(s)$, its derivatives $p_2'(s)$ and $p_2''(s)$, and the corresponding function $d_p(s)$, are plotted in Fig. 1. It is easy to verify that the function $d_p(s) = p_2'(s)/s$ satisfies

$$|d_p(s)| < 1, \quad \text{for all } s \in (0, \infty) \tag{17}$$

and

$$\lim_{s \to 0} d_p(s) = \lim_{s \to \infty} d_p(s) = 1. \tag{18}$$

Therefore, we have

$$|\mu d_p(|\nabla \phi|)| \le \mu$$

which verifies the boundedness of the diffusion rate for the potential $p = p_2$.

The sign of the function $d_p(s)$ for $p = p_2(s)$, as plotted in Fig. 1(d), indicates the property of the FAB diffusion in the following three cases:

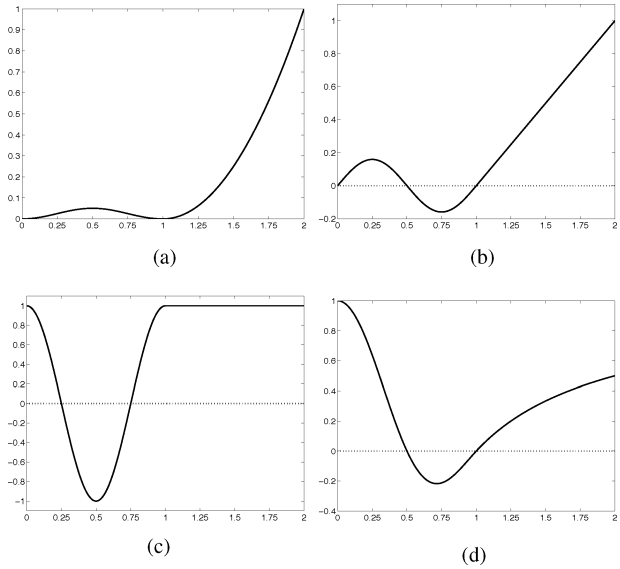

Fig. 1. Double-well potential $p = p_2(s)$ and its first derivative p_2' and second derivative p_2'', and corresponding function $d_p(s)$ are shown in (a), (b), (c), and (d), respectively.

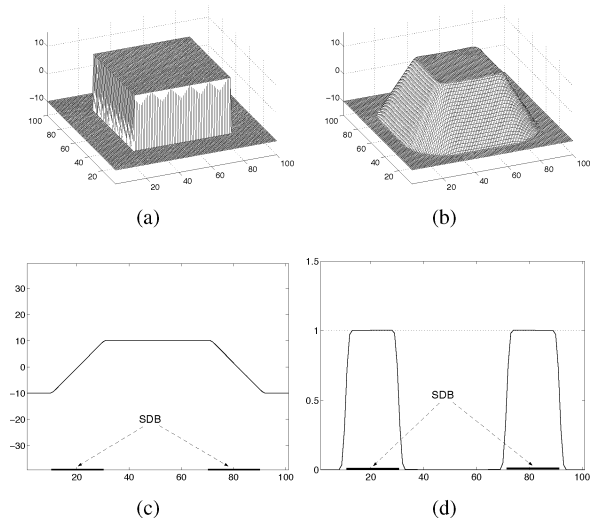

Fig. 2. Distance regularization effect on binary step function with the double-well potential $p = p_2(s)$. (a) Initial LSF ϕ_0. (b) Final LSF ϕ after the evolution. (c) and (d) Show a cross section of ϕ and $|\nabla\phi|$ for the final function ϕ, respectively.

- for $|\nabla\phi| > 1$, the diffusion rate $\mu d_p(|\nabla\phi|)$ is positive, and the diffusion (14) is forward, which decreases $|\nabla\phi|$;
- for $(1/2) < |\nabla\phi| < 1$, the diffusion rate $\mu d_p(|\nabla\phi|)$ is negative, and the diffusion becomes backward, which increases $|\nabla\phi|$;
- for $|\nabla\phi| < (1/2)$, the diffusion rate $\mu d_p(|\nabla\phi|)$ is positive, and the diffusion (14) is forward, which further decrease $|\nabla\phi|$ down to zero.

The key differences between the FAB diffusions with potentials p_1 and p_2 are the boundedness of the corresponding diffusion rate and the diffusion behavior for the case $|\nabla\phi| < (1/2)$, as can be seen from the previous descriptions for both cases.

D. Distance Regularization Effect

We demonstrate the distance regularization effect of DRLSE by simulating the FAB diffusion (14) with the initial function ϕ_0 being a binary step function. The binary step function ϕ_0 is defined by

$$\phi_0(\mathbf{x}) = \begin{cases} -c_0, & \text{if } \mathbf{x} \in R_0 \\ c_0, & \text{otherwise} \end{cases} \tag{19}$$

where $c_0 > 0$ is a constant, and R_0 is a region in the domain Ω. Despite the irregularity of the binary step function, the FAB diffusion (14) is able to evolve the LSF into a function with desired regularity. It is worth noting that a binary step function can be generated extremely efficiently. Such initialization is desirable in many practical applications for its computational efficiency and simplicity, as will be demonstrated in an application of DRLSE for image segmentation in Section III.

The effect of the distance regularization with the double-well potential $p = p_2(s)$ can be seen from the following numerical simulation of the FAB diffusion (14). We used a binary step function ϕ_0 on a 100×100 grid, as defined by (19), with the region R_0 being a rectangle. To test the regularization effect of the FAB diffusion in DRLSE, we used a large $c_0 = 10$ in (19) to create a particularly steep shape of ϕ_0 at the zero crossing, as shown in Fig. 2(a). The final function ϕ of the diffusion is shown in Fig. 2(b), which exhibits the shape of a signed distance function in a band around the zero level set and a flat shape outside the band. We call this band a signed distance band (SDB). The width of the SDB is controlled by the constant c_0. This is because, when the function ϕ becomes a signed distance function in the SDB, its values vary from $-c_0$ to c_0 across the band at a rate of $|\nabla\phi| = 1$. This implies that the width of the SDB is approximately $2c_0$.

The evolution from a binary step function to the function of the previously described profile is described as follows. At the zero crossing of the binary step function ϕ_0, the values of $|\nabla\phi_0|$ are larger than 1 due to a sharp jump from $-c_0$ to c_0. As a result, the diffusion rate $\mu d_p(|\nabla\phi|)$ is positive and, therefore, the diffusion (14) is forward, which keeps decreasing the gradient magnitude $|\nabla\phi|$ until it approaches 1. The decreasing of $|\nabla\phi|$ is stopped when it reaches 1, otherwise, the FAB diffusion (14) would become backward and, therefore, increases $|\nabla\phi|$ back to 1, because the diffusion rate $\mu d_p(|\nabla\phi|)$ is negative for $(1/2) < |\nabla\phi| < 1$. As a result, the function ϕ converges to a signed distance in a band around its zero level set, i.e., the previously mentioned SDB. On the two sides of the SDB, $|\nabla\phi|$ is initially 0, which indicates that the diffusion rate $\mu d_p(|\nabla\phi|) \geq 0$. Therefore, the diffusion (14) is forward, which keeps the function ϕ flat on the two sides of the SDB. The signed distance property of the final function ϕ near the zero level set can be seen more clearly from 1-D cross sections of the $\phi(x, y)$ and its gradient magnitude $|\nabla\phi(x, y)|$. Fig. 2(c) and (d) shows 1-D cross sections of $\phi(x, y)$ and $|\nabla\phi(x, y)|$, respectively, for $y = 50$. In the SDB, the values of $|\nabla\phi|$ are sufficiently close to 1, as shown in Fig. 2(d).

The advantage of the double-well potential p_2 over the simple potential p_1 can be clearly seen when a binary step function is used as the initial function. For the binary initial function, we have $|\nabla\phi| = 0$ in the interior of the regions $\{\phi_0 = c_0\}$ and $\{\phi_0 = -c_0\}$. Thus, the FAB diffusion with $p = p_1$ is backward

diffusion with an arbitrarily large diffusion rate. In this case, the strong backward diffusion drastically increases $|\nabla\phi|$ and cause oscillation in ϕ, which finally appears as periodic "peaks" and "valleys" in the converged LSF. Although these "peaks" and "valleys" appear at a certain distance to the zero level set, they may slightly distort the zero level contour. This undesirable side effect can be avoided by using the double-well potential $p = p_2$, as described previously.

E. Finite Difference Scheme

The DRLSE in (13) can be implemented with a simple finite difference scheme as follows. We consider the 2-D case with a time dependent LSF $\phi(x, y, t)$. The spatial derivatives $\partial\phi/\partial x$ and $\partial\phi/\partial y$ in our model are approximated by the central difference. We use fixed space steps $\triangle x = \triangle y = 1$ for computing spatial derivatives. The temporal partial derivative $\partial\phi/\partial t$ is approximated by the forward difference. The time dependent LSF $\phi(x, y, t)$ is given in discretized form $\phi^k_{i,j}$ with spatial index (i, j) and temporal index k. Then, the level set evolution equation is discretized as the following finite difference equation $(\phi^{k+1}_{i,j} - \phi^k_{i,j})/\Delta t = L(\phi^k_{i,j})$, where $L(\phi^k_{i,j})$ is the approximation of the right hand side in the evolution equations. This equation can be expressed as

$$\phi^{k+1}_{i,j} = \phi^k_{i,j} + \Delta t L\left(\phi^k_{i,j}\right), \qquad k = 0, 1, 2, \ldots \tag{20}$$

which is an iteration process used in the numerical implementation of DRLSE.

Given spacial steps $\triangle x = \triangle y = 1$, the choice of the time step for this finite difference scheme must satisfy the Courant-Friedrichs-Lewy (CFL) condition $\mu\Delta t < (1/4)$ for numerical stability (see Appendix A). In practice, one can use a relatively large time step $\Delta t > 1$ to speed up the curve evolution, in which case the parameter μ must be relatively small to meet the CFL condition.

It is worth noting that, although the FAB diffusion term in DRLSE is derived from the proposed variational level set formulation in (4), we believe that it can be incorporated into more general level set evolution equations that are not necessarily derived from a variational formulation. For example, consider a typical level set evolution equation in conventional level set formulation

$$\frac{\partial\phi}{\partial t} = F|\nabla\phi| + A \cdot \nabla\phi \tag{21}$$

where F is a scalar function and A is a vector valued function. In standard numerical solution to this PDE, spatial derivatives are discretized by upwind scheme [20]. Central difference scheme is not stable for this PDE.

Adding the distance regularization term into the PDE, the level set evolution in (21) becomes a DRLSE formulation

$$\frac{\partial\phi}{\partial t} = \mu\mathrm{div}(d_p(|\nabla\phi|)\nabla\phi) + F|\nabla\phi| + A \cdot \nabla\phi. \tag{22}$$

Due to the added distance regularization term, all the spatial derivatives in (22) can be descretized by central difference scheme, and the corresponding numerical scheme is stable without the need for reinitialization. It is well known that the central difference scheme is more accurate and efficient than the first-order upwind scheme that is commonly used in conventional level set formulations.

III. Application to Image Segmentation

The general DRLSE formulation in (4) can be used in various applications with different definitions of the external energy $\mathcal{E}_{\mathrm{ext}}$. For image segmentation applications, a variety of image information, including region-based or edge-based image formation, can be used to define the external energy. In this section, we only provide an application of DRLSE to an active contour model using edge-based information in the external energy, as a demonstration of the effectiveness of the general DRLSE formulation.

A. Edge-Based Active Contour Model in Distance Regularized Level Set Formulation

Let I be an image on a domain Ω, we define an edge indicator function g by

$$g \triangleq \frac{1}{1 + |\nabla G_\sigma * I|^2} \tag{23}$$

where G_σ is a Gaussian kernel with a standard deviation σ. The convolution in (23) is used to smooth the image to reduce the noise. This function g usually takes smaller values at object boundaries than at other locations.

For an LSF $\phi : \Omega \to \Re$, we define an energy functional $\mathcal{E}(\phi)$ by

$$\mathcal{E}(\phi) = \mu\mathcal{R}_p(\phi) + \lambda\mathcal{L}_g(\phi) + \alpha\mathcal{A}_g(\phi) \tag{24}$$

where $\lambda > 0$ and $\alpha \in \Re$ are the coefficients of the energy functionals $\mathcal{L}_g(\phi)$ and $\mathcal{A}_g(\phi)$, which are defined by

$$\mathcal{L}_g(\phi) \triangleq \int_\Omega g\delta(\phi)|\nabla\phi|d\mathbf{x} \tag{25}$$

and

$$\mathcal{A}_g(\phi) \triangleq \int_\Omega gH(-\phi)d\mathbf{x} \tag{26}$$

where δ and H are the Dirac delta function and the Heaviside function, respectively.

With the Dirac delta function δ, the energy $\mathcal{L}_g(\phi)$ computes the line integral of the function g along the zero level contour of ϕ. By parameterizing the zero level set of ϕ as a contour $C : [0, 1] \to \Omega$, the energy $\mathcal{L}_g(\phi)$ can be expressed as a line integral $\int_0^1 g(\mathcal{C}(s))|\mathcal{C}'(s)|ds$. The energy $\mathcal{L}_g(\phi)$ is minimized when the zero level contour of ϕ is located at the object boundaries. Note that the line integral $\int_0^1 g(\mathcal{C}(s))|\mathcal{C}'(s)|ds$ was first introduced by Caselles *et al.* as an energy of an parameterized contour $\mathcal{C}$ in their proposed geodesic active contour (GAC) model [11].

The energy functional $\mathcal{A}_g(\phi)$ computes a weighted area of the region $\Omega^-_\phi \triangleq \{\mathbf{x} : \phi(\mathbf{x}) < 0\}$. For the special case $g = 1$, this energy is exactly the area of the region Ω^-_ϕ. This energy $\mathcal{A}_g(\phi)$ is introduced to speed up the motion of the zero level contour in the level set evolution process, which is necessary when the initial contour is placed far away from the desired object boundaries. In this paper, we use LSFs that take negative values inside the zero level contour and positive values outside.

In this case, if the initial contour is placed outside the object, the coefficient α in the weighted area term should be positive, so that the zero level contour can shrink in the level set evolution. If the initial contour is placed inside the object, the coefficient α should take negative value to expand the contour. From the level set evolution given in (30), we can see that the role of g in this energy term $\mathcal{A}_g$ is to slow down the shrinking or expanding of the zero level contour when it arrives at object boundaries where g takes smaller values.[1]

In practice, the Dirac delta function δ and Heaviside function H in the functionals $\mathcal{L}_g$ and $\mathcal{A}_g$ are approximated by the following smooth functions δ_ε and H_ε as in many level set methods [20], [30], defined by

$$\delta_\varepsilon(x) = \begin{cases} \frac{1}{2\varepsilon}\left[1+\cos\left(\frac{\pi x}{\varepsilon}\right)\right], & |x| \le \varepsilon \\ 0, & |x| > \varepsilon \end{cases} \tag{27}$$

and

$$H_\varepsilon(x) = \begin{cases} \frac{1}{2}\left(1+\frac{x}{\varepsilon}+\frac{1}{\pi}\sin\left(\frac{\pi x}{\varepsilon}\right)\right), & |x| \le \varepsilon \\ 1, & x > \varepsilon \\ 0, & x < -\varepsilon. \end{cases} \tag{28}$$

Note that δ_ε is the derivative of H_ε, i.e., $H'_\varepsilon = \delta_\varepsilon$. The parameter ε is usually set to 1.5.

With the Dirac delta function δ and Heaviside function H in (25) and (26) being replaced by δ_ε and H_ε, the energy functional $\mathcal{E}(\phi)$ is then approximated by

$$\mathcal{E}_\varepsilon(\phi) = \mu\int_\Omega p(|\nabla\phi|)\,d\mathbf{x} + \lambda\int_\Omega g\delta_\varepsilon(\phi)|\nabla\phi|\,d\mathbf{x} + \alpha\int_\Omega g H_\varepsilon(-\phi)\,d\mathbf{x}. \tag{29}$$

This energy functional (29) can be minimized by solving the following gradient flow:

$$\frac{\partial\phi}{\partial t} = \mu\,\mathrm{div}\left(d_p(|\nabla\phi|)\nabla\phi\right) + \lambda\delta_\varepsilon(\phi)\mathrm{div}\left(g\frac{\nabla\phi}{|\nabla\phi|}\right) + \alpha g\delta_\varepsilon(\phi) \tag{30}$$

given an initial LSF $\phi(\mathbf{x},0) = \phi_0(\mathbf{x})$. The first term on the right hand side in (30) is associated with the distance regularization energy $\mathcal{R}_p(\phi)$, while the second and third terms are associated with the energy terms $\mathcal{L}_g(\phi)$ and $\mathcal{A}_g(\phi)$, respectively. Equation (30) is an edge-based geometric active contour model, which is an application of the general DRLSE formulation (13). For simplicity, we refer to this active contour model as a DRLSE model in this section and Section IV.

B. Narrowband Implementation

The computational cost of a level set method can be greatly reduced by confining the computation to a narrowband around the zero level set. For conventional level set formulations, the narrowband implementation requires even more frequent reinitialization [31] or an additional step of velocity extension [32], adding further sophistication in the implementation. For the DRLSE formulation, neither reinitialization nor velocity extension procedures are needed in the narrowband implementation due to the intrinsic distance regularization effect in the level set evolution. The narrowband implementation of DRLSE is simple and straightforward, in which the iteration process only consists of updating the LSF according to the difference equation (20) and constructing the narrowband, as described in the following. Moreover, the narrowband implementation of the DRLSE model (30) allows the use of a large time step in the finite difference scheme to significantly reduce the number of iterations and computation time, as in its full domain implementation.

We denote by $\phi_{i,j}$ an LSF defined on a grid. A grid point (i,j) is called a zero crossing point, if either $\phi_{i-1,j}$ and $\phi_{i+1,j}$ are of opposite signs or $\phi_{i,j-1}$ and $\phi_{i,j+1}$ are of opposite signs. The set of all the zero crossing points of the LSF is denoted by Z. Then, we construct the narrowband as

$$B_r = \bigcup_{(i,j)\in Z} N_{i,j}^{(r)} \tag{31}$$

where $N_{i,j}^{(r)}$ is a $(2r+1)\times(2r+1)$ square block centered at the point (i,j). We can set r to be the smallest value $r=1$, in which case the narrowband B_r is the union of the 3×3 neighborhoods of the zero crossing points.

The narrowband implementation of the DRLSE consists of the following steps:

Step 1) **Initialization**. Initialize an LSF ϕ to a function ϕ_0. Then, construct the initial narrowband $B_r^0 = \bigcup_{(i,j)\in Z^0} N_{i,j}^{(r)}$, where Z^0 is the set of the zero crossing points of ϕ^0.

Step 2) **Update the LSF**. Update $\phi_{i,j}^{k+1} = \phi_{i,j}^k + \tau L(\phi_{i,j}^k)$ on the narrowband B_r^k as in (20).

Step 3) **Update the narrowband**. Determine the set of all the zero crossing pixels of $\phi_{i,j}^{k+1}$ on B_r^k, denoted by Z^{k+1}. Then, update the narrowband by setting $B_r^{k+1} = \bigcup_{(i,j)\in Z^{k+1}} N_{i,j}^{(r)}$.

Step 4) **Assign values to new pixels on the narrowband**. For every point (i,j) in B_r^{k+1} but not in B_r^k, set $\phi_{i,j}^{k+1}$ to h if $\phi_{i,j}^k > 0$, or else set $\phi_{i,j}^{k+1}$ to $-h$, where h is a constant, which can be set to $r+1$ as a default value.

Step 5) **Determine the termination of iteration**. If either the zero crossing points stop varying for m consecutive iterations or k exceeds a prescribed maximum number of iterations, then stop the iteration, otherwise, go to Step 2.

The readers are referred to our conference paper [33] for more details in the narrowband implementation of the level set formulation in our preliminary work [27].

C. Initialization of Level Set Function

The DRLSE not only eliminates the need for reinitialization, but also allows the use of more general functions as the initial LSFs. We propose to use a binary step function in (19) as the initial LSF, as it can be generated extremely efficiently. Moreover, the region R_0 in (19) can sometimes be obtained by a simple and efficient preliminary segmentation step, such as thresholding, such that R_0 is close to the region to be segmented. Thus, only

[1]The function g in the energy $\mathcal{A}_g$ can be replaced by a different function f defined by other types of image information, such as region-based information, which can take positive and negative values, thereby allowing bidirectional motion (i.e., shrinking or expanding at different locations) of the contour in a single process of curve evolution.

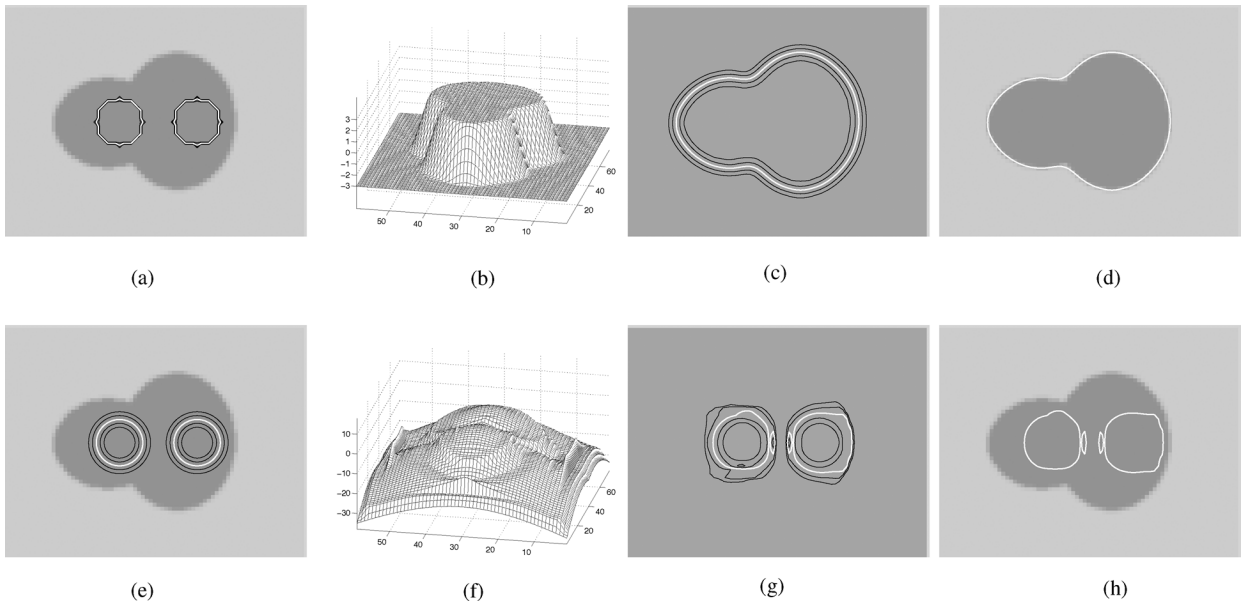

Fig. 3. Behavior of level set evolution in the DRLSE model (upper row) and GAC model (lower row). The LSF in the DRLSE model evolves from a binary step function ϕ_0^{drlse} to a function ϕ^{drlse} with desirable regularity, as shown in (b); the LSF in the GAC model evolves from a signed distance function ϕ_0^{gac} to an LSF ϕ^{gac} with irregularities, as shown in (f). (a) Isocontours of the initial LSF ϕ_0^{drlse} (a binary step function). (b) Converged LSF ϕ^{drlse} of the DRLSE model. (c) Isocontours of ϕ^{drlse} at levels $-2, -1$, 0, 1, and 2. (d) Zero level contour of the LSF ϕ^{drlse} overlaid on the image. (e) Isocontours of the initial LSF ϕ_0^{gac} (a signed distance function). (f) LSF ϕ^{gac} after 50 iterations in the GAC model. (g) Isocontours of ϕ^{gac} at levels $-2, -1$, 0, 1, and 2. (h) Zero level contour of ϕ^{gac} overlaid on the image.

a small number of iterations are needed to move the zero level set from the boundary of R_0 to the desired object boundary.

As explained in Section II-D, the LSF evolves from a binary step function to an approximate signed distance function on an SDB around the zero level set, and the width of the SDB is about $2c_0$. In practice, the image domain is a discrete grid, and the SDB should have at least one grid point on each side of the zero level contour. Therefore, we suggest that c_0 be chosen from the range $c_0 \geq 1$. In this paper, we usually set $c_0 = 2$ for the definition of the binary step function in (19) as the initial LSF, unless otherwise specified.

IV. Experimental Results

This section shows the results of the DRLSE model (30) for both synthetic and real images. There are parameters λ, μ, and α in this model, and the time step Δt for the implementation. The model is not sensitive to the choice of λ and μ, which can be fixed for most of applications. The choice of the parameter μ is subject to the CFL condition described in Section II-E. Unless otherwise specified, these parameters are fixed as $\lambda = 5.0$, $\mu = 0.04$, and $\Delta t = 5.0$ in this paper.

The parameter α needs to be tuned for different images. A nonzero α gives additional external force to drive the motion of the contour, but the resulting final contour may slightly deviate from the true object boundary due to the shrinking or expanding effect of the weighted area term. To avoid such deviation, one can refine the final contour by further evolving the contour for a few iterations with the parameter $\alpha = 0$. For images with weak object boundaries, a large value of α may cause boundary leakage, i.e., the active contour may easily pass through the object boundary. Therefore, for images with weak object boundaries, the value of α should be chosen relatively small to avoid boundary leakage.

We first demonstrate the level set regularization effect of the distance regularization term by applying the DRLSE model (30) to a synthetic image shown in Fig. 3. To show the advantage of the DRLSE formulation, we also applied the well-known GAC model [11] to this image, and compared the behaviors of the level set evolution in the two formulations. The level set evolution in the GAC model is

$$\frac{\partial \phi}{\partial t} = g|\nabla \phi| \mathrm{div}\left(\frac{\nabla \phi}{|\nabla \phi|}\right) + \nabla g \cdot \nabla \phi + \alpha g |\nabla \phi| \qquad (32)$$

where α is a constant, which plays a similar role as the parameter α in the DRLSE model (30), and g is the edge indicator function defined by (23).

In this experiment, we set $\Delta t = 1.0$, $\mu = 0.2$, $\lambda = 5$, and $\alpha = -3.0$ for the DRLSE model, and the time step $\Delta t = 0.2$ and $\alpha = -0.3$ for the GAC model. We generated a signed distance function ϕ_0^{gac} as the initial LSF for the GAC model. To see the behavior of the level set evolution (32) in the GAC model, we applied it without using reinitialization in this experiment. To demonstrate the regularization effect of the DRLSE formulation, we used a binary step function defined by $\phi_0^{\mathrm{drlse}} = c_0 \mathrm{sign}(\phi_0^{\mathrm{gac}})$, with $c_0 = 3$, as the initial LSF for the DRLSE model, which has discontinuity at the zero crossing. The isocontours of these two initial LSFs ϕ_0^{drlse} and ϕ_0^{gac} at levels $-2, -1$, 0, 1, and 2 are overlaid on the image, as shown in Fig. 3(a) and (e).

Despite the discontinuity of the binary step function ϕ_0^{drlse} as the initial LSF, the DRLSE model is able to regularize the LSF, and thereby maintain stable level set evolution and ensure accurate computation. Fig. 3(b) shows the LSF of the DRLSE model

after 240 iterations. This LSF exhibits the shape of a signed distance function in a vicinity of the zero level set, and a flat shape outside the vicinity. The regularity of the LSF can be also seen from its isocontours. Fig. 3(c) shows five isocontours at levels $-2, -1$, 0, 1, and 2 of the LSF given by the DRLSE model, with the white contour being the zero level contour and the black contours being the other four isocontours. The signed distance property of this LSF can be seen from the uniform distances between isocontours, as shown in Fig. 3(c). With an intrinsic capability of distance regularization, the DRLSE model is able to evolve the LSF stably, while moving the zero level set toward the desired object boundary, as shown in Fig. 3(d).

By contrast, the level set evolution in the GAC model constantly degrades the LSF, from a nice signed distance function to a function with undesirable irregularities. Fig. 3(f) shows the LSF after 50 iterations of the GAC model, denoted by ϕ^{gac}, which exhibits very steep shape in some regions and very flat shape in other regions. The irregularities of the LSF ϕ^{gac} can be clearly seen from its isocontours at levels of $-2, -1$, 0, 1, and 2, as shown in Fig. 3(g). The isocontours are densely distributed in regions where the LSF is too steep, and are sparsely distributed in regions where the LSF is too flat. Such irregularities of the LSF causes numerical errors in the computation involving the derivatives of the LSF, and further iteration of the LSF will further degrade the LSF, which would finally destroy the stability of the level set evolution. The degraded LSF has to be "repaired" by replacing it with a signed distance function for further computation. This is why reinitialization is required in conventional level set formulations as a numerical remedy to maintain the regularity of the LSF. In all the experiments in the following, reinitialization is applied periodically when the GAC model is used for comparison with the DRLSE model.

While reinitialization can be used as a numerical remedy to maintain the regularity of the LSF in conventional level set formulations, it inevitably introduces additional numerical errors, which can be quite considerable if it is used inappropriately. This is shown in the following experiment. We apply the DRLSE model in (30) and the GAC model on synthetic images and compare the accuracy of the segmentation results. The true object boundaries are known for the synthetic images, which can be used to quantitatively evaluate the accuracy of the segmentation results. A metric to evaluate the accuracy of a segmentation result is the mean error defined by $e(C) = (1/N)\sum_{n=1}^{N} \text{dist}(P_i, S)$, where C is a contour as the segmentation result, S is the true object contour, $P_1, \ldots, P_N$ are the points on the contour C, and $\text{dist}(P_i, S)$ is the distance from the point P_i to the contour S.

We applied the DRLSE model and the GAC model to the synthetic images in Fig. 4(a)–(c), each with a star-shaped object, whose boundary is known and used as the ground truth. We used the same initial contour for both models. In this experiment, we use $\alpha = 1.0$ and a large time step $\Delta t = 5.0$ in our model (30). It is worth noting that our method is not sensitive to the choice of the parameter μ. This is demonstrated by applying the DRLSE model with two different values of $\mu = 0.04$ and $\mu = 0.004$. The mean errors of the corresponding results for the three images are shown as the lighter bars in Fig. 4(d). For each image, the two results of the DRLSE model with the two

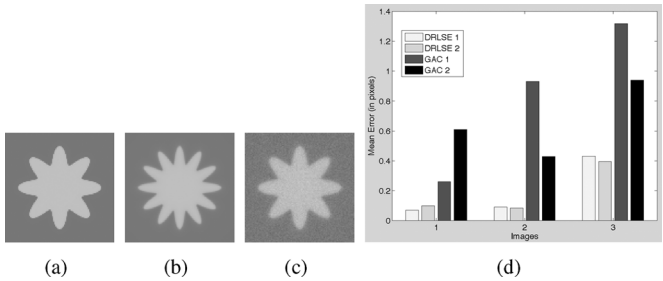

Fig. 4. Comparison of the DRLSE model and the GAC model on three synthetic images in (a), (b), and (c). For each images, the mean errors of the DRLSE model with $\mu = 0.04$ and 0.004 are shown as the two lighter bars in (d), and the GAC model with reinitialization at every five iterations and at every ten iterations are shown as the two darker bars in (d).

different values of μ are quite close to each other, with very similar mean errors. All the mean errors for the three images are below 0.5 pixels, as shown in Fig. 4(d).

For the GAC model, we use the time step $\Delta t = 0.5$. The coefficients of the balloon force in the GAC model (32) is set to $\alpha = 0.2$. We obtained two results for each image by applying the GAC model: one is obtained with reinitializations at every five iterations, and the other with reinitializations at every ten iterations. In this experiment, the reinitialization for the GAC model is performed by solving the PDE (3) with 20 iterations (more iterations may cause larger displacement of the zero level contour). The mean errors of the corresponding results for the three images are shown as the darker bars in Fig. 4(d). For each image, the two result of the GAC model with the two frequencies of applying reinitialization are somewhat different, with the corresponding mean errors larger than those of the DRLSE model. From this experiment, we can see that the errors of the GAC model become larger when reinitialization is applied more frequently. The mean error for the image in Fig. 4(c) is larger than one pixel when reinitialization is applied at every five iterations. This reveals a difficulty in applying reinitialization in conventional level set formulations: while reinitialization is required to reshape the degraded LSF periodically, too frequently applying it may cause considerable error. There is no general answer to the problem of choosing an appropriate frequency of applying reinitialization. Therefore, reinitialization is often applied in an ad-hoc manner in the implementation of conventional level set methods. There is no such issue in the implementation of the proposed DRLSE formulation, and the numerical accuracy is ensured by the intrinsic distance regularization on the LSF.

The DRLSE model (30) has been applied to real images. For examples, Fig. 5 shows the results of the DRLSE model for five real images: a CT image with a tumor (the dark area) in human liver, an image of a pot, a microscope image of cells, an image of a T-shaped object, and an MR image of a human bladder. For this experiment, we used the narrowband implementation of the DRLSE model as described in Section III-B, with the smallest parameter $r = 1$ in the construction of the narrowband as in (31). We recorded the CPU times consumed for the five images. In this experiment, the narrowband algorithm is implemented by a C program in MEX format, which was compiled and run in Matlab. The CPU times were obtained by running the program on a Lenovo ThinkPad notebook with Intel (R) Core (TM) 2

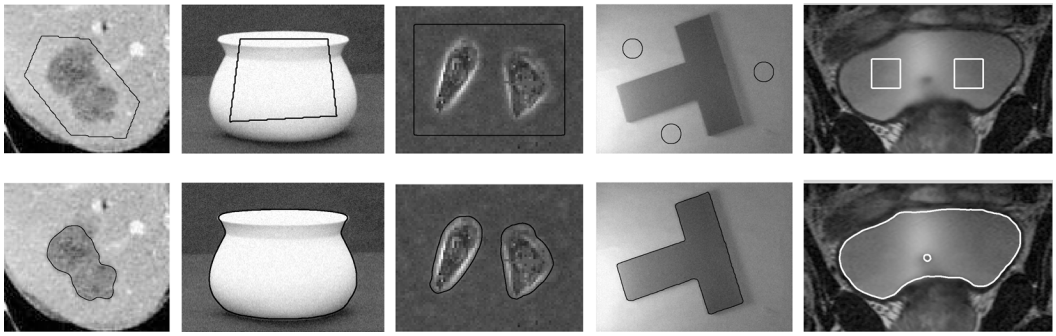

Fig. 5. Results of narrowband implementation of the DRLSE model for five real images, with CPU times 0.12, 0.36, 0.09, 0.92, and 0.23 s consumed for the images from left to right. Upper row: Input images and initial contours. Lower row: segmentation results.

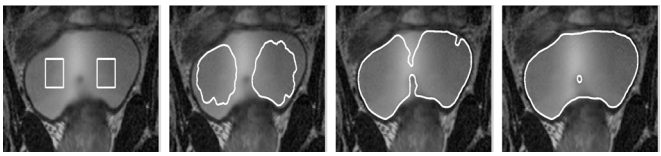

Fig. 6. Curve evolution in the narrowband implementation of the DRLSE model for an MR image of bladder. The initial contour, and the contours at iterations 50, 140, and 220 are shown from left to right.

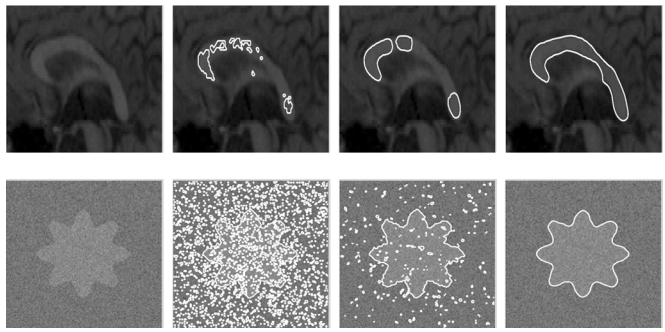

Fig. 7. Results of the DRLSE model in narrowband implementation using initialization from thresholding. Column 1: the input images. Column 2: the initial contours obtained by thresholding on the input image. Column 3: intermediate contours, after ten iterations for the upper image and one iteration for the lower image. Column 4: the final contours, after 110 iterations for the upper image and five iterations for the lower image.

Duo CPU, 2.40 GHz, 2 GB RAM, with Matlab 7.4 on Windows Vista. The upper row of Fig. 5 shows the initial contours overlaid on the five images. We used the same time step $\Delta t = 5.0$ and chose the parameter α as 2.5, -4.0, 1.5, -5.0, -3.0 for these images (from left to right). The corresponding results of the DRLSE model are shown in the lower row. The sizes of the five images, from left to right, are 110×112, 148×202, 65×83, 192×254, and 107×180 pixels, and the corresponding CPU times consumed by our algorithm are 0.12, 0.36, 0.09, 0.92, and 0.23 s, respectively. To show the curve evolution process of the DRLSE model, we display the zero level contours at the iterations 50, 140, and 220 for the MR image in Fig. 6.

To compare the computation speeds of the DRLSE model and the GAC model, we applied them to the same images, with the same initial contours in Fig. 5. For simplicity and fair comparison, we use the full domain implementation of both models in pure Matlab. The results of the full domain implementation of the DRLSE model are sufficiently close to those of the narrowband implementation shown in Fig. 5. By choosing appropriate parameters for the GAC model and applying fast marching algorithm for reinitialization, we obtained similar results as those of the DELSE model shown in Fig. 5. The CPU times consumed by the DRLSE model for the five images, from left to right: 3.41, 15.25, 1.48, 32.67, and 8.54 s, and the corresponding CPU time consumed by the GAC model are 22.98, 173.71, 11.34, 215.42, and 80.22 s, respectively. Obviously, the DRLSE model is significantly faster than the GAC model. This is mainly due to the fact that the DRLSE model does not need reinitialization and allows the use of a larger time step, which significantly reduces the number of iterations and computation time. It is worth noting that computational efficiency advantage of the DRLSE formulation over conventional level set formulations would be even more obvious in narrowband implementations, as the latter typically require even more frequent reinitializations or additional numerical tricks, such as velocity extension.

As mentioned in Section III-C, the binary initial LSF can be obtained efficiently by applying thresholding or other simple and efficient methods as preliminary segmentation on the input image. Fig. 7 shows the results of the DRLSE model in narrowband implementation for an MR image of a human brain (the corpus callosum is the object to be segmented) in the upper row and a synthetic noisy image in the lower row. We apply thresholding on the input image to obtain the region R_0 for the definition of the initial LSF ϕ_0 in (19). Column 2 of Fig. 7 shows the zero level contours of the initial level set function ϕ_0, and Columns 3 and 4 show intermediate contours and the final contours, respectively. In this experiment, the parameter α is set to -2.0 and 0 for the images in the upper and lower rows, respectively. It is worth noting that binary initial LSF ϕ_0 for the synthetic noisy image is highly irregular, and so are the zero level contours, as shown in Column 2. Despite the initial severe irregularity, the LSF is quickly regularized in the level set evolution due to the distance regularization term in the DRLSE model. The regularity of the LSF is significantly improved after only one iteration, with more regular zero level contours as shown in Column 3. After five iterations, the LSF exhibits desirable regularity and zero level contour converges to the desired object boundary, as shown in Column 4. The whole iteration process only took 0.02 s for this image with 128×128 pixels.

V. Conclusion

We have presented a new level set formulation, which we call DRLSE. The proposed DRLSE formulation has an intrinsic capability of maintaining regularity of the level set function, particularly the desirable signed distance property in a vicinity of the zero level set, which ensures accurate computation and stable level set evolution. DRLSE can be implemented by a simpler and more efficient numerical scheme than conventional level set methods. DRLSE also allows more flexible and efficient initialization than generating a signed distance function as the initial LSF. As an application example, we have applied DRLSE to an edge-based active contour model for image segmentation, and provided a simple and efficient narrowband implementation of this model. This active contour model in DRLSE formulation allows the use of relatively large time steps to significantly reduce iteration numbers and computation time, while maintaining sufficient numerical accuracy in both full domain and narrowband implementations, due to the intrinsic distance regularization embedded in the level set evolution. Given its efficiency and accuracy, we expect that the proposed distance regularized level set evolution will find its utility in more applications in the area of image segmentation, as well as other areas where level set method has been and could be applied.

Appendix A
Further Analysis of the Fab Diffusion

To further understand the property of the diffusion (14), we decompose the divergence on the right hand as a weighted sum of the second derivatives of ϕ in the tangential and normal directions to the isophote lines (i.e., isocontours). The readers are referred to [28, p.65] for such a decomposition formula. We denote by T and N the tangential direction and normal direction, respectively. The second derivatives of ϕ in the T-direction and the N-direction are denoted by ϕ_{TT} and ϕ_{NN}, respectively. Thus, the diffusion (14) can be rewritten as

$$\frac{\partial \phi}{\partial t} = c_T(|\nabla\phi|)\phi_{TT} + c_N(|\nabla\phi|)\phi_{NN} \tag{33}$$

where $c_T(s) = \mu d_p(s)$ and $c_N(s) = \mu p''(s)$. The signs of the coefficients $c_T(|\nabla\phi|)$ and $c_N(|\nabla\phi|)$ determine whether the diffusion in the tangential and normal directions is forward or backward.

In particular, for the potential $p = p_2(s)$, both coefficients c_T and c_N are positive for $|\nabla\phi| > 1$ or $0 < |\nabla\phi| < (1/4)$ and, therefore, the diffusion (14) is forward. In the case of $(1/4) < |\nabla\phi| < 1$, either c_T or c_N is negative and, therefore, the diffusion (14) is backward in the tangential or normal direction. Moreover, we have the following important properties:

$$|c_T(s)| \le \mu, \quad \text{and} \quad |c_N(s)| \le \mu. \tag{34}$$

Furthermore, by L'Hospital's rule, we have

$$\lim_{s\to 0+} c_T(s) = \lim_{s\to 0+} c_N(s) = \lim_{s\to\infty} c_T(s) = \lim_{s\to\infty} c_N(s) = \mu$$

The boundedness of the coefficients c_T and c_N allows the use of a fixed and relatively large time step in an finite difference scheme. This can be seen from the Courant–Friedrichs–Lewy (CFL) condition for the finite difference schemes. From the decomposition (33), we have the CFL condition as $\Delta t \le h^2/(4\max\{|c_N|, |c_T|\})$ for fixed space steps $\Delta x = \Delta y = h$. Note that this CFL condition appeared in [34] in the context of image denoising using a FAB diffusion. This CFL condition and the boundedness of c_N and c_T in (34) imply that a fixed time step can be used in the finite difference scheme for the diffusion equation (14) with $p = p_2(s)$, as long as $\mu\Delta t \le h^2/4$. If the coefficients c_T and c_N are not bounded, then the time step (inversely proportional to c_T and c_N) has to be sufficiently small to satisfy the CFL condition and, therefore, more iterations are needed to obtain converged result. This will make the algorithm more time-consuming.

Acknowledgment

The authors would like to thank S. Zhou for discussion on nonlinear diffusion, K. Konwar for his contribution in developing the narrowband implementation of the proposed algorithm, and J. Macione, L. He, X. Han, and M. Rousson for their helpful comments and proofreading.

References

[1] S. Osher and J. Sethian, "Fronts propagating with curvature-dependent speed: Algorithms based on Hamilton-Jacobi formulations," *J. Comput. Phys.*, vol. 79, no. 1, pp. 12–49, Nov. 1988.

[2] A. Dervieux and F. Thomasset, "A finite element method for the simulation of Rayleigh-Taylor instability," *Lecture Notes Math.*, vol. 771, pp. 145–158, 1980.

[3] A. Dervieux and F. Thomasset, "Multifluid incompressible flows by a finite element method," *Lecture Notes Phys.*, vol. 141, pp. 158–163, 1980.

[4] V. Caselles, F. Catte, T. Coll, and F. Dibos, "A geometric model for active contours in image processing," *Numer. Math.*, vol. 66, no. 1, pp. 1–31, Dec. 1993.

[5] R. Malladi, J. A. Sethian, and B. C. Vemuri, "Shape modeling with front propagation: A level set approach," *IEEE Trans. Pattern. Anal. Mach. Intell.*, vol. 17, no. 2, pp. 158–175, Feb. 1995.

[6] M. Kass, A. Witkin, and D. Terzopoulos, "Snakes: Active contour models," *Int. J. Comput. Vis.*, vol. 1, no. 4, pp. 321–331, Jan. 1987.

[7] C. Xu, A. Yezzi, and J. Prince, "On the relationship between parametric and geometric active contours," in *Proc. 34th Asilomar Conf. Signals, Syst., Comput.*, Pacific Grove, CA, Oct. 2000, pp. 483–489.

[8] S.-C. Zhu and A. Yuille, "Region competition: Unifying snakes, region growing, and Bayes/MDL for multiband image segmentation," *IEEE Trans. Pattern. Anal. Mach. Intell.*, vol. 18, no. 9, pp. 884–900, Sep. 1996.

[9] C. Xu and J. Prince, "Snakes, shapes, and gradient vector flow," *IEEE Trans. Imag. Process.*, vol. 7, no. 3, pp. 359–369, Mar. 1998.

[10] S. Kichenassamy, A. Kumar, P. Olver, A. Tannenbaum, and A. Yezzi, "Gradient flows and geometric active contour models," in *Proc. 5th Int. Conf. Comput. Vis.*, 1995, pp. 810–815.

[11] V. Caselles, R. Kimmel, and G. Sapiro, "Geodesic active contours," *Int. J. Comput. Vis.*, vol. 22, no. 1, pp. 61–79, Feb. 1997.

[12] R. Kimmel, A. Amir, and A. Bruckstein, "Finding shortest paths on surfaces using level set propagation," *IEEE Trans. Pattern Anal. Mach. Intell.*, vol. 17, no. 6, pp. 635–640, Jun. 1995.

[13] C. Samson, L. Blanc-Feraud, G. Aubert, and J. Zerubia, "A variational model for image classification and restoration," *IEEE Trans. Pattern Anal. Mach. Intell.*, vol. 22, no. 5, pp. 460–472, May 2000.

[14] N. Paragios and R. Deriche, "Geodesic active contours and level sets for detection and tracking of moving objects," *IEEE Trans. Pattern Anal. Mach. Intell.*, vol. 22, no. 3, pp. 266–280, Mar. 2000.

[15] T. Chan and L. Vese, "Active contours without edges," *IEEE Trans. Image Process.*, vol. 10, no. 2, pp. 266–277, Feb. 2001.

[16] C. Li, C. Kao, J. C. Gore, and Z. Ding, "Minimization of region-scalable fitting energy for image segmentation," *IEEE Trans. Image Process.*, vol. 17, no. 10, pp. 1940–1949, Oct. 2008.
[17] D. Cremers, "A multiphase levelset framework for variational motion segmentation," *Scale Space Meth. Comput. Vis.*, pp. 599–614, June 2003.
[18] H. Jin, S. Soatto, and A. Yezzi, "Multi-view stereo reconstruction of dense shape and complex appearance," *Int. J. Comput. Vis.*, vol. 63, no. 3, pp. 175–189, July 2005.
[19] J. Sethian, *Level Set Methods and Fast Marching Methods*. Cambridge, U.K.: Cambridge Univ. Press, 1999.
[20] S. Osher and R. Fedkiw, *Level Set Methods and Dynamic Implicit Surfaces*. New York: Springer-Verlag, 2002.
[21] M. Sussman, P. Smereka, and S. Osher, "A level set approach for computing solutions to incompressible two-phase flow," *J. Comput. Phys.*, vol. 114, no. 1, pp. 146–159, Sep. 1994.
[22] M. Sussman and E. Fatemi, "An efficient, interface-preserving level set redistancing algorithm and its application to interfacial incompressible fluid flow," *SIAM J. Sci. Comput.*, vol. 20, no. 4, pp. 1165–1191, Jul. 1999.
[23] D. Peng, B. Merriman, S. Osher, H. Zhao, and M. Kang, "A PDE-based fast local level set method," *J. Comput. Phys.*, vol. 155, no. 2, pp. 410–438, Nov. 1999.
[24] G. Barles, H. M. Soner, and P. E. Sougandis, "Front propagation and phase field theory," *SIAM J. Control Optim.*, vol. 31, no. 2, pp. 439–469, Mar. 1993.
[25] J. Gomes and O. Faugeras, "Reconciling distance functions and level sets," *J. Vis. Commun. Image Represent.*, vol. 11, no. 2, pp. 209–223, Jun. 2000.
[26] M. Weber, A. Blake, and R. Cipolla, "Sparse finite elements for geodesic contours with level-sets," in *Proc. Eur. Conf. Comput. Vis.*, 2004, pp. 391–404.
[27] C. Li, C. Xu, C. Gui, and M. D. Fox, "Level set evolution without re-initialization: A new variational formulation," in *Proc. IEEE Conf. Comput. Vis. Pattern Recognit.*, 2005, vol. 1, pp. 430–436.
[28] G. Aubert and P. Kornprobst, *Mathematical Problems in Image Processing: Partial Differential Equations and the Calculus of Variations*. New York: Springer-Verlag, 2002.
[29] L. Evans, *Partial Differential Equations*. Providence, RI: Amer. Math. Soc., 1998.
[30] H. Zhao, T. Chan, B. Merriman, and S. Osher, "A variational level set approach to multiphase motion," *J. Comput. Phys.*, vol. 127, no. 1, pp. 179–195, Aug. 1996.
[31] D. Adalsteinsson and J. Sethian, "A fast level set method for propagating interfaces," *J. Comput. Phys.*, vol. 118, no. 2, pp. 269–277, May 1995.
[32] D. Adalsteinsson and J. Sethian, "The fast construction of extension velocities in level set methods," *J. Comput. Phys.*, vol. 148, no. 1, pp. 2–22, Jan. 1999.
[33] C. Li, C. Xu, K. Konwar, and M. D. Fox, "Fast distance preserving level set evolution for medical image segmentation," in *Proc. 9th Int. Conf. Control Autom. Robot. Vis.*, 2006, pp. 1–7.
[34] G. Gilboa, N. Sochen, and Y. Zeevi, "Forward-and-backward diffusion processes for adaptive image enhancement and denoising," *IEEE Trans. Image Process.*, vol. 11, no. 7, pp. 689–703, Jul. 2002.

Chunming Li received the B.S. degree in mathematics from Fujian Normal University, Fujian, China, the M.S. degree in mathematics from Fudan University, Shanghai, China, and the Ph.D. degree in electrical engineering from University of Connecticut, Storrs, CT, in 2005.

He was a Research Fellow at the Vanderbilt University Institute of Imaging Science, Nashville, TN, from 2005 to 2009. He is currently a Researcher in medical image analysis at the University of Pennsylvania, Philadelphia. His research interests include image processing, computer vision, and medical imaging, with expertise in image segmentation, MRI bias correction, active contour models, variational and PDE methods, and level set methods. He has served as referee and committee member for a number of international conferences and journals in image processing, computer vision, medical imaging, and applied mathematics.

Chenyang Xu (S'94–M'01–SM'06) received the B.S. degree in computer science and engineering from the University of Science and Technology of China, Hefei, in 1993 and the M.S.E. and Ph.D. degrees in electrical and computer engineering from the Johns Hopkins University, Baltimore, MD, in 1995 and 1999, respectively.

In 2000, he joined the Siemens Corporate Research, Princeton, NJ, as a member of technical staff. From 2006 to 2009, he was a Program Manager responsible for multimodality image fusion and image-guided solutions for interventional imaging applications. During the same time period, he was the cofounder and the codirector of the Siemens Center for Medical Imaging Validation (CMIV), Beijing, China. Since July 2009, he has been the Chief Technology Officer at the Siemens Technology-To-Business (TTB) Center, Berkeley, CA. His research interests include image segmentation and registration, shape representation and analysis, deformable models, graph-based algorithms, statistical validation, and their applications in medical imaging, particularly intervention and minimal invasive surgery. He is both the co-inventor and the technical manager of the world's first commercial 3-D imaging-guidance technology product for treating complex heart arrhythmias, CARTOMERGE.

Dr. Xu was the recipient of the Frost Sullivan's 2006 Excellence in Technology Award.

Changfeng Gui received the B.S. and M.S. degrees in mathematics from Peking University, Beijing, China, and the Ph.D. degree in mathematics at the University of Minnesota, Minneapolis, in 1991.

He is currently a Professor in the Department of Mathematics, the University of Connecticut, Storrs. His research interests include nonlinear partial differential equations, applied mathematics, and image processing.

Dr. Gui was a recipient of Andrew Aisensdadt Prize, Centre de Recherches Mathematiques, Canada, in 1999, and PIMS Research Prize, Pacific Institute of Mathematical Sciences, in 2002.

Martin D. Fox (S'69–M'73) received the B.E.E. degree from Cornell University, Ithaca, NY, in 1969, the Ph.D. Degree from Duke University, Durham, NC, in 1972, and the M.D. degree from University of Miami, Coral Gables, in 1983.

He has published extensively in the areas of Medical Imaging and Biomedical Engineering. He has taught at the University of Connecticut, Storrs, since 1972 where he is presently a Professor of Electrical and Computer Engineering. His research interests include ultrasound imaging and Doppler, microcontroller based devices, biomedical instrumentation, and multidimensional image processing.